Conference on Modelling Fluid Flow (CMFF'22)
The 18th International Conference on Fluid Flow Technologies
Budapest, Hungary, August 30 -September 2, 2022

AEROACOUSTIC NOISE REDUCTION OF OPEN PHOTOACOUSTIC CELLS SUPPORTED BY EXPERIMENTS AND SIMULATIONS

Miklós BALOGH[1], Gábor KOSCSÓ[2], Bálint KOCSIS[3], Csaba HORVÁTH[4], Zoltán BOZÓKI[5]

[1] Corresponding Author. Department of Fluid Mechanics, Faculty of Mechanical Engineering, Budapest University of Technology and Economics. Bertalan Lajos u. 4 – 6, H-1111 Budapest, Hungary. Tel.: +36 1 463 1560, E-mail: balogh.miklos@gpk.bme.hu
[2] Department of Fluid Mechanics, Faculty of Mechanical Engineering, Budapest University of Technology and Economics. E-mail: koscso@ara.bme.hu
[3] Department of Fluid Mechanics, Faculty of Mechanical Engineering, Budapest University of Technology and Economics. E-mail: kocsis.balint@gpk.bme.hu
[4] Department of Fluid Mechanics, Faculty of Mechanical Engineering, Budapest University of Technology and Economics. E-mail: horvath.csaba@gpk.bme.hu
[5] University of Szeged, Faculty of Science and Informatics, Department of Optics and Quantum Electronics. E-mail: zbozokiphysx.u-szeged.hu

ABSTRACT

In this study aeroacoustic investigations have been carried out in order to further develop the critical components of a quick responding, open, continuously measured detection cell based photoacoustic (PA) measurement system, in order to reduce the aeroacoustic noise. This is a key aspect to operate the recently developed open PA cell under high velocity throughflow conditions. As compared to other, sampling-based PA systems, the photoacoustic component of the newly developed instrument presented herein is better integrated, significantly reduced in weight and size, and the gas flowrate that can be analysed is several orders of magnitude higher. A good aeroacoustic design is extremely important for an open PA cell, since significant acoustic noise can be generated even at relatively low flow rates, which drastically reduces the signal-to-noise ratio of the concentration measurements. The geometric constraints of the PA measurement system also must be considered. In addition, the structure must be sufficiently rigid so that the interactions between velocity fluctuations and the solid body do not cause mechanical vibrations. The new method has been developed to provide an improved aeroacoustic. Both numerical and experimental investigations have been carried out for the verification of this new method.

Keywords: Computational Aero-Acoustics (CAA), Computational Fluid Dynamics (CFD), Detached Eddy Simulation (DES), noise reduction, OpenFOAM, photoacoustic (PA) measurements

NOMENCLATURE

p_0	[Pa]	reference pressure
T_0	[K]	reference temperature
ρ_0	[kg/m^3]	reference density
ν	[m^2/s]	kinematic viscosity
a	[m/s]	speed of sound
Ma	[-]	Mach number

1. INTRODUCTION

In order to gain a deeper understanding of the operation of the system and to better understand the aeroacoustic noise generation mechanisms in the system (those noise sources which originate from the flow), we need to become acquainted with the basics of photoacoustic spectroscopy and the aeroacoustic problems affecting the system. Photoacoustic spectroscopy is a technique that detects acoustic waves generated from thermal de-excitation of molecules or particles upon absorption of modulated electromagnetic radiation, namely light used to generated by lasers. This technique provides high sensitivity and selectivity, furthermore large dynamic detection range making it suitable for trace gas applications [1,2,3]. Acoustic resonators are used to further increase the sensitivity of the photoacoustic (PA) signals. The modulation frequency of the electromagnetic radiation is matched to an acoustic eigenfrequency of the resonator thus exciting the corresponding acoustic mode. Conventional photoacoustic spectroscopy usually applies closed resonators, where gaseous samples are filled into a sealed resonator, but the sensitivity of measurements from closed resonators is limited [4]. Open resonators eliminate this limited sensitivity and have the additional advantage of enabling continuous exchange of gas between resonator and environment, which is particularly useful for continuous PA measurement. Experts working on the development of the present system have played a significant role in the research and development of measurement systems with short-response open chambers [5]. One can read more about the theory of photoacoustic measurements in the work of Miklós et al. [6] and in the article of Dumitras et al. [7]. modelled and numerically examined photoacoustic resonators. The numerical examination and modelling of PA cells is discussed e.g. in the paper of Baumann et al. [8], while a shape optimization study is presented by Kost et al. [9]. Until now, the study of the flow and aeroacoustic properties of photoacoustic resonators has not been a primary aspect in the international literature, and therefore personal consultations held with the leading experts in the field of photoacoustics have been key to determining which direction to go.

As compared to other photoacoustic (PA) systems used to date, the photoacoustic component of the instrument developed herein must be better integrated, significantly reduced in size and weight, and be well designed concerning the suppression of aeroacoustic noise sources. As the gas flow rates in earlier applications of the PA method have been several orders of magnitude lower than in the current application, their aerodynamic and resultant aeroacoustic designs have not been suitable, i.e. significant aeroacoustic noise is generated even at relatively low flow rates. The aerodynamic noise at low frequencies is such that it mechanically overdrives the microphone, which thus becomes insensitive at the higher resonance frequency. As a result, such designs cannot be used in the open, continuously measured detection cell based PA measurement system at higher flow rates, and new solutions need to be researched and developed.

Our main goal in this investigation was to solve the problems arising when using PA measurement methods at higher flow rates, namely to reduce the amplitude of aeroacoustics noise at low frequencies, in order to avoid the mechanical overload of the in-built microphones.

For this reason, the available design was investigated experimentally and with numerical simulations, which confirmed our first conjecture that the design should be reviewed and modified. A new cell design is proposed to ensure simultaneously isokinetic sampling and reliable and accurate operation even at high flow rates. The essence of this design is that the gas to be tested flows freely through the streamlined resonator, without significant contraction. The prototype performed better in experimental tests, but it was also limited to a lower flow rate than required. A final optimized version is designed and tested with numerical simulations.

The evaluation showed that the low frequency noise is reduced thanks to the new design, while isokinetic sampling is fulfilled as well.

2. INVESTIGATION OF THE ORIGINAL PA MEASUREMENT SYSTEM

To assess the condition of the original PA measurement system and analyse the original geometry, data was provided by the Department of Optics and Quantum Electronics, University of Szeged. The goal of the investigation was mainly to localize the aeroacoustic noise sources. This was realized by empirical and theoretical methods, and numerical simulations. The examined original open PA cell construction is shown in Figure 1.

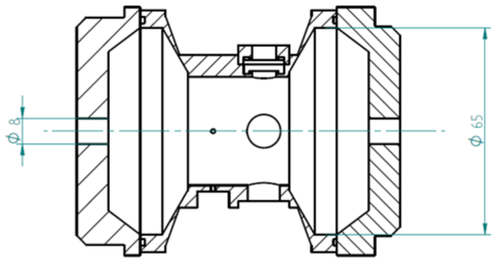

Figure 1. Cross-section of the investigated original PA cell

The following sections will discuss the conclusions drawn as a result of the empirical, theoretical and numerical investigations.

2.1. Empirical and theoretical considerations

The following potential noise sources related to the original cell design were identified based on the vast aerodynamic and aeroacoustic experience of the research team:

- The flow entering the open PA cell through the small inlet cross-section cannot follow the sudden cross-sectional expansion. This results in a free jet. As a result, vortices are generated in the shear layer of the free jet, which create additional noise sources on the exit side of the open PA cell, as the vortices interact with surfaces.
- The medium, acting as a free jet, does not fill the entire volume of the resonator, inducing a secondary flow that appears as a toroidal vortex with a flow velocity. This can cause problems when measuring concentrations, as it significantly increases the residence time.
- Recesses in the resonator wall (microphone neck, laser window) can act as a driven cavity or resonator.

2.2. Preliminary numerical simulations

To support the empirical and theoretical considerations, numerical simulations are performed with a simplified model of the chamber construction under investigation. A block structured mesh was generated in a way to satisfy the requirements of low-Reynolds wall treatment (y+ < 1) results in a fairly high resolution forming 407k cells for a quarter section of the original geometry, assuming tangential periodicity. The geometry was created using proprietary software along with the software Gmsh [10]. The numerical grid (hereinafter referred to as "mesh"), which is the basis of spatial discretization, was constructed with Gmsh as well. Since the problems to be solved are primarily due to microphone overdrive caused by low-frequency noise, we mainly focused on examining the low frequency noise. According to that and considering that the Mach number is fairly low (Ma < 0.05), an incompressible approach to aeroacoustics is applied using aeroacoustic analogies. The numerical simulations were performed in three steps using the OpenFOAM toolbox [11]. In order to model fully developed flow at the inlet, while omitting the need for the approximately one meter long preparatory pipe section (significantly reducing computational costs) a steady state precursor simulation was run, which consisted of an axially periodic domain modelling the long pipe section. The volume flow rate was set to 30 l/min, which corresponds to an average velocity of 10.01 m/s on the inlet side, as earlier measurement experience showed that the aeroacoustic noise was significant at this operation point. During the precursor simulations, the Launder-Sharma k-epsilon turbulence model with a low Reynolds wall function was used, which provides a formalism resolving the laminar sublayer next to the wall. The simulations have been carried out under the ambient conditions corresponding to the planned measurements in the anechoic room. This implies a reference pressure of p_0 = 101325 Pa, a reference temperature of T_0 = 293K, resulting a density of ρ_0 = 1.204 kg m^{-3}, a kinematic viscosity of ν = 1.5e-5 m^2 s^{-1}, and a speed of sound of a = 343 m/s. These reference values were used in all the subsequent simulations.

In the next step, the initial conditions for the time resolved simulations were generated by running a steady state simulation over the entire geometry, using the results of the precursor simulation for the inlet boundary condition.

In the last step, a time resolved simulation was run using the initial and boundary conditions generated by the previous simulations. From the results of the steady state simulations, the time resolved boundary conditions were determined by the Divergence-Free Synthetic Eddy Method [12]. Due to the fine mesh resolution, we utilized a hybrid technique combining the advantages of Large Eddy Simulation and Reynolds averaged models, namely the Spalart-Allmaras DES (Detatched Eddy Simulation) model. In this model, sub-grid turbulence is modelled by the Spalart-Allmaras turbulence model, while in parts of the range where mesh resolution allows, turbulent structures (large vortices) are explicitly simulated. During the simulation, the pressure and the Curle pressure were sampled. The latter is calculated based on the Curle analogy, which is a formal solution to the Lighthill analogy with respect to solid surfaces.

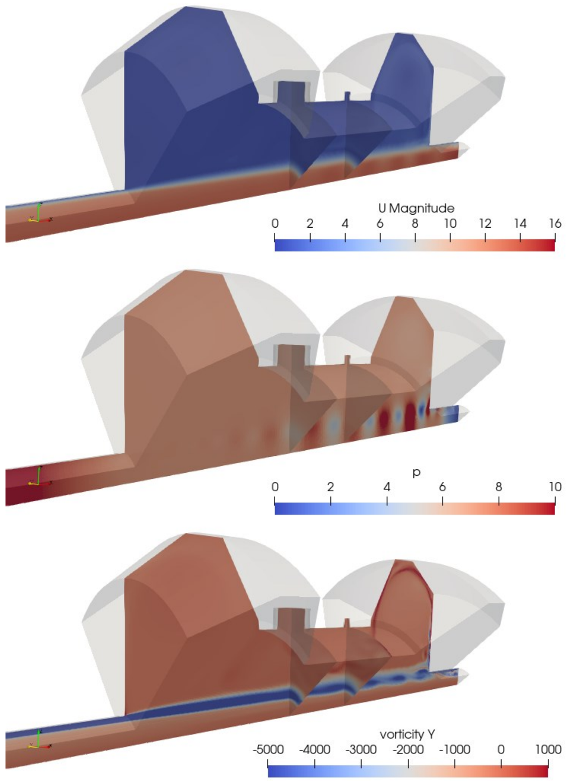

Figure 2. Simulated instantaneous values of velocity magnitude (top), relative pressure (middle), y-component of vorticity (bottom) for the original PA cell.

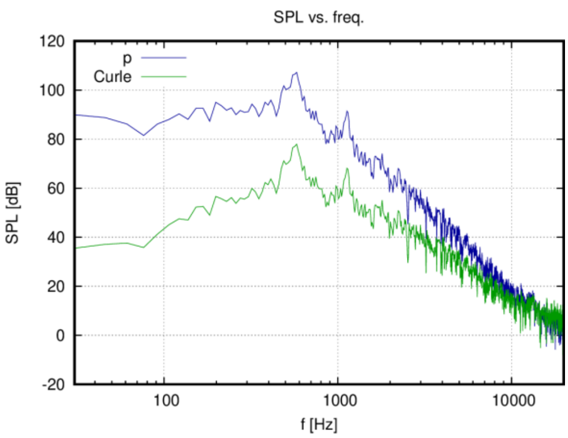

Figure 3. Sound pressure level based on relative pressure and Curle pressure.

Figure 2 shows the vortices generated in the shear layer of the free jet, which impinge on the walls of expansion chamber at the junction of the outlet nozzle. The sound pressure levels calculated from the sampled values of pressure and Curle pressure are shown in Figure 3. The simulations confirmed the conclusions drawn from the empirical considerations that the flow in the PA cell results in a free jet due to the rather sudden cross-sectional changes. The vortices, generated periodically in the shear layer of the free jet and their interactions with the can generates a significant amount of aeroacoustic noise. This makes the given design unacceptable for use as a PA cell, due to the high levels of low frequency noise. This design therefore needs to be further developed.

2.3. Proposal for modified photoacoustic chamber geometry

Studies on the original chamber geometry have shown that sudden changes in cross-sectional area have a negative effect on the aeroacoustic properties of the cell, i.e. they can significantly increase the noise, thus mechanically overdriving the microphone making it impossible to detect the photoacoustic signal. The small inflow cross-section results in a significantly higher velocity at a given volume flow rate, thus a higher Reynolds number, i.e. a more turbulent and at the same time noisier flow. As the goal is to reduce the aeroacoustic noise of the photoacoustic chamber, it is important to introduce the medium into the resonator with the largest possible cross-section and with the least possible change of direction and diameter. In the proposed design shown in Fig. 4, the measuring cell, through which the total amount of gas flows, is optimally connected to the piping in which the concentration of a given substance is to be measured. The microphones and laser are introduced through streamlined supports holding the photoacoustic chamber in the axis of the piping.

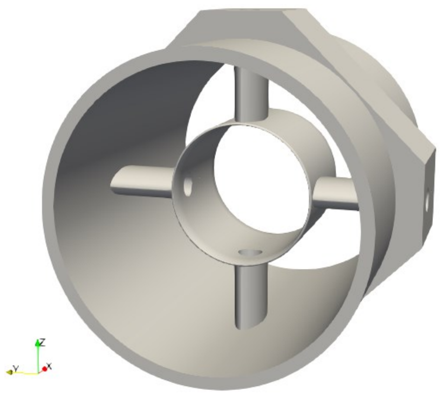

Figure 4. Initially proposed PA chamber design with streamlined resonator and supports (struts).

3. INVESTIGATION OF THE INITIALLY PROPOSED AND IMPROVED OPEN PA CELL GEOMETRIES

3.1. Laboratory measurements

Detailed laboratory measurements were performed in the anechoic room of the Békésy György Acoustic Research Laboratory, the aim of which was to become better familiarized with the acoustic characteristics of the proposed photoacoustic chamber design. Brüel & Kjaer microphone (type 4165) and its electronics (type 2639 preamplifier, type 2636 amplifier) were used during the measurements as reference. The acoustic signals were measured with Knowles SPU0410HR5H-PB MEMS microphones with their dedicated electronics developed by VIDEOTON. The data series are collected with a Lenovo Thinkpad 20C6-00LLHV laptop via the National Instruments NI-9234 dynamic signal acquisition module mounted in an NI cDAQ-9178 chassis.

The measurements were carried out at seven different flow velocities (4, 5.9, 7.5, 8.6, 10.6, 11.9 and 15 m/s) with a sampling frequency of 51.2 kHz. The following conclusions were drawn from the measurements:

- The free jet noise is frequency dependent and does not include contamination from the rpm or blade passing frequency of the air supply system.
- Base noise is particularly common at higher frequencies.
- The generated noise is proportional to the power of 6.27 of the flow velocity, characteristic of predominantly dipole sound generation.
- There is no resonance at 12.5 kHz, which is the eigenfrequency of the PA resonator. The resonance excited by the flow avoids this mode.
- At higher frequencies, the background noise is lower, so it is advisable to keep the frequency of the PA measurements in this range.

3.2. Numerical investigation of the proposed PA cell geometry: geometry and mesh

As a first step in the examination of noise reduction solutions, a numerical investigation of the flow in the proposed prototype was performed.

Based on the CAD files of the prototype, a block-structured approach was used which provided a mesh of very high quality using Gmsh. Thanks to the planes of symmetry of the geometry, only a quarter of the entire PA cell was modelled, which consisted of 620 rectangular blocks. A boundary layer mesh was created which was parametrized based on the expected magnitudes of the investigated velocities.

3.3. Numerical investigation of the proposed PA cell geometry: simulation

In accordance with the methodology applied in section 2.2, the numerical simulations in phase two were also performed in three steps. In the steady state precursor simulations, the flow was driven by a pressure gradient, which was iteratively tuned as a function of the desired volume flow rate. In this way, it was possible to set volume flow rates equal to those recorded during the measurements, while keeping the numerical costs low. The volume flow rates that were investigated ~ 212 and 848 l/min, which correspond to average velocities of 1 and 4 m/s, respectively.

In the second step, the initial conditions were generated by running steady state simulations as well. In the third and final step, time resolved simulations were run using the initial and boundary conditions generated by the simulations in steps one and two. During the transient simulations, the time step was determined to allow the description of phenomena up to 20 kHz. Due to the high sampling frequency, it was not possible to save and store all the spatial data, and therefore only those that were essential for the evaluation were extracted during the simulations. The simulations were run on 32-thread (16-core) processors. Instantaneous states are shown in Figure 5.

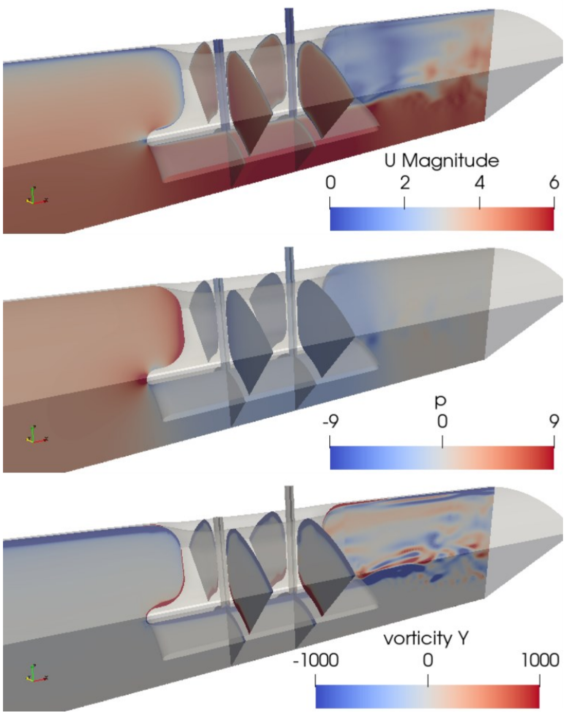

Figure 5. Instantaneous values of velocity magnitude (top), relative pressure (middle), y-component of vorticity (bottom) for the initially proposed PA cell, for a volume flow rate of 848 l/min.

4. ENHANCED DESIGN OF THE PHOTOACOUSTIC CHAMBER GEOMETRY

As it is expected and shown by the previous simulation results, perturbations increase with increasing Reynolds number. While at lower Reynolds numbers the flow shows an orderly picture, at higher values, the disorder due to turbulence is significant, both on the inlet side as well as downstream of the photoacoustic chamber. This turbulent flow is the primary source of noise that makes measurements difficult, and therefore needs to be reduced. A simple means of reducing the Reynolds number is to increase the diameter of the enclosing pipe section. Our experience from the measurements has shown that the generated noise is proportional to the flow velocity raised to the power of 6.27. Therefore, for a given volume flow rate, increasing the diameter will result in a significant reduction of noise.

4.1 A designing method for improving PA cells at higher flow rates

A proper design of the resonator tube and mounting pylons is also key in preventing the noise generation from suppressing the photoacoustic signal.

Geometric constraints important from a photoacoustic point of view must also be taken into account during the design. Such constraints include the cylindrical internal geometry of the resonator tube and the need for introducing/extracting optical and acoustic signals to/from the resonator tube via internal passages in the mounting pylons. In addition, the structure must be sufficiently rigid so that the interactions between flow disturbances (vortices) and the solid body do not cause mechanical vibrations. Table 1 below summarizes the direction in which the various aspects influence the design of the structure.

Table 1. Constraints influencing the design of the photoacoustic chamber

	Photoacoustics	Mechanics	Aeroacoustics
Resonator tube	Regular, cylindrical design	Maximize wall thickness	Minimize sudden change in diameter, minimize wall thickness
Mounting support structures	Minimum required cross-section for optical and acoustic signals	Maximize wall thickness	Minimize relative thickness and streamlined design

The method we have developed results in an aeroacoustically improved design based on the geometrical constraints coming from photoacoustics as well as mechanical considerations. An iterative procedure finds the optimum, which is illustrated in the following steps:

Step 0: Input data (diameter, length and wall thickness of the resonator tube, radius of inlet and outlet edge rounding, diameter and position of optical and acoustic lines along the longitudinal axis of the resonator tube, minimum required wall thickness of the pylons).

Step 1: Based on the given data, the leading edge region of the resonator pipe is designed from a lower and an upper chamber segment using the shape functions of a NACA00XX airfoil.

Step 2: The trailing edge region of the resonator tube is designed similarly to Step 1.

Step 3: The cross section of the pylon (strut) is also designed as a NACAXX00 airfoil with the largest possible chord length, taking into account the shortening caused in step 1 and 2, and the fillet radius of the pylon - resonator tube interference. In this step, the trailing edge is at a fixed location along the longitudinal axis of the resonator tube, the position of the leading edge is changed iteratively, until the maximum relative thickness of the profile reaches a minimum. During the iteration, the minimum distance between the optical and acoustic channels and the envelope curve of the airfoil is equal to the specified minimum wall thickness.

Step 4: Design of the pylon - resonator tube interference. This is the second-order continuous interference (fillet) between the pylon and the resonator tube, where the function describing the transition is defined by a circular arc with the specified fillet radius.

4.2. Numerical investigation of the improved PA design

After performing the shape optimization of the chamber under the current geometric constraints, we carried out simulations according to the simulation methodology described earlier in this chapter. Figure 6 show that the flow disturbance was reduced thanks to the improved design.

A quantitative evaluation of the simulation results was performed using the measurements described at the beginning of this chapter. Since the minimum velocity for which measurements were carried out was 4 m/s, only the corresponding simulation results of ~848 l/min were compared. The Sound Pressure Level (SPL) results of the comparison are illustrated in Figure 7.

Composite SPL were calculated by summing the time series values of the Curle pressure fluctuations and the static pressures, which were used for verification purposes. These results systematically overestimate the measurements by 24 dB. The reason for the discrepancy is that the simulations were carried out for a closed tube section, while the measurements were carried with a free space downstream of the PA cell. Sampling took place in this free space, and therefore a systematic deviation of 24 dB between measurements and simulations is absolutely realistic. The composite results show that shape optimization is effective in reducing the low frequency noise generated by the photoacoustic chamber.

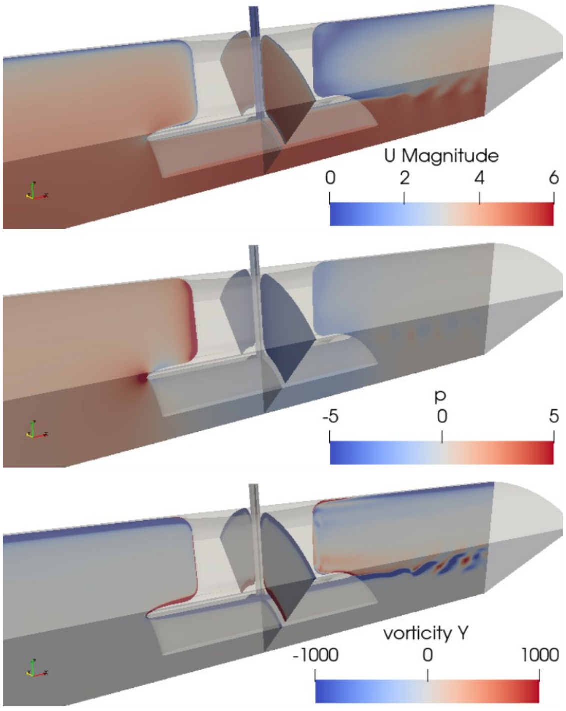

Figure 6. Instantaneous values of velocity magnitude (top), relative pressure (middle), y-component of vorticity (bottom) for the closed PA cell, for a volume flow rate of 848 l/min.

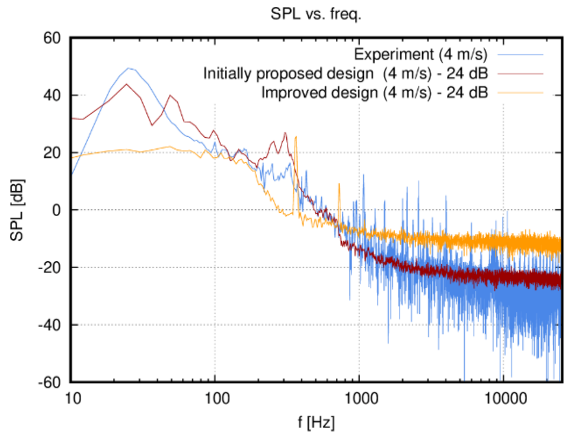

Figure 7. Frequency spectrum of measured and simulated sound pressure levels.

5. NUMERICAL SIMULATIONS TO DETERMINE THE RESIDENCE TIME DISTRIBUTION

One of the main advantages of using an open photoacoustic chamber for isokinetic sampling is that the resonator can be placed in the piping which is transporting the gas to be measured. As a result, the concentration in the gas flowing through the open chamber is the same as that measured in the piping, as it is not necessary to install a deflection or passive/active sampling mechanism. The quality of the isokinetic samples can be determined by investigating the residence time distribution (RTD). For this purpose, numerical simulations with additional passive scalar transport were performed.

The same geometry and mesh used for these calculations as in the former simulations.

For the transient RTD simulations, the time step was chosen so that the Courant number would fall within the appropriate range, which requires it to be kept below 1. Though less stringent than the requirements enforced during the acoustic simulations, even this is a very small time step, and it was not possible to save and store all the spatial data. During the transient flow simulation, passive scalar transport was also activated, taking into account turbulent diffusion, where scalar diffusivity was calculated from turbulent viscosity.

Volume averages were calculated for the inlet and outlet cross-sections of the domain and for the centre plane of the laser beam, which were saved for each time step. The volume average of the scalar passing through the resonator and that of the entire cross-section in the plane of the laser beam was monitored separately. The passive scalar concentration introduced at the inlet varied over time according to a square pulse. The square pulse turned on the scalar source for one tenths of a second from 0.3 seconds to 0.4 seconds. The simulations ran for 4-8 days on 32-thread (16-core) processors, depending on which Reynolds number was being investigated.

Residence Time Distributions (RTD) were evaluated at the inlet, the outlet, and in the plane of the laser beam. The inner cross-section of the resonator, the entire cross-section of the piping and the opening for the laser was monitored separately.

Figure 8. provide information regarding the reference (ideal) residence time distributions (dashed line), along with the outcomes of the simulations (solid lines). Each cross-section is marked with its own colour. The inlet is marked with blue, the inner cross-section of the resonator is denoted with green, the entire cross-section is marked with red, and the outlet cross-section denoted with light blue. Orange indicates the concentration of the scalar mixing into the passage of the microphone within the mounting pylon. Due to the turbulent mixing and the deceleration in the boundary layer, the pulse shapes become more and more adherent to the lognormal distribution away from the inlet. However, in the inner cross-section of the photoacoustic chamber a distribution similar to the source pulse is obtained. This proves that isokinetic sampling is guaranteed with the optimized open chamber design.

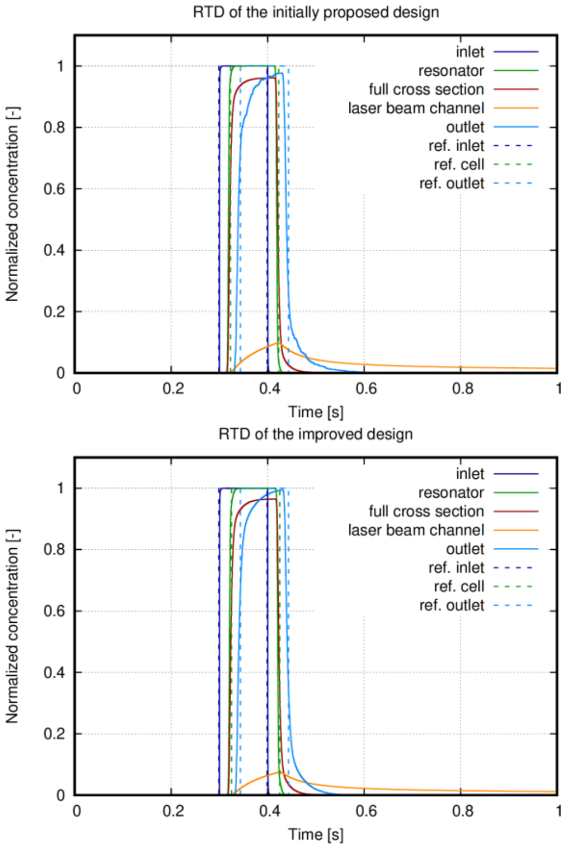

Figure 8. The Residence Time Distribution (RTD) in the investigated cross-sections at a volume flow rate of 848 l/min for the initially proposed PA design (top) and for the improved PA (bottom).

6 CONCLUSIONS

In this study, aeroacoustic investigations had been carried out in order to further develop the critical components of a quick responding, open, continuously measured detection cell based photoacoustic (PA) measurement system, in order to reduce the aeroacoustic noise. The actual design of the measurement system is investigated first. Aerodynamic and aeroacoustic analysis is performed for the existing geometry based on empirical and theoretical considerations along with numerical simulations in order to support the proposition of a quiet geometry. We identified qualitative noise reduction trends and proposed a new design on behalf of the photoacoustic chamber to reduce the aeroacoustic noise and increase the signal-to-noise ratio. These investigations were supplemented with measurements.

During the next phase of the development, we performed aerodynamic and aeroacoustic analysis on the geometry proposed during the initial phase. We have developed a shape optimization method that takes into account geometric and photoacoustic constraints, based on which the PA design can be further refined. The initially proposed and the further improved PA design was investigated with numerical simulations. The simulation results were compared to the results of the measurements carried out in the acoustic laboratory. A systematic deviation of 24 dB was experienced between the measurements and simulations, but the course of the spectra is very similar. The simulations performed with the improved design resulted in lower sound pressure levels than simulations performed on the initially proposed geometry in the critical low frequency range.

In order to prove the suitability of the new PA design for isokinetic sampling, RTD analysis is performed for each geometry. Based on the results, it can be concluded that both the initially proposed and improved photoacoustic chamber design meets the requirements set for isokinetic sampling, as the peak concentration of the gas flowing through the photoacoustic chamber is nearly equal to the average concentration entering the entire cross-section in the flow normal plane at the location of the laser beam.

ACKNOWLEDGEMENTS

This work has been supported by the Hungarian National Research, Development and Innovation Centre under contract No. K 138176. The research reported in this paper and carried out at BME has been supported by the NRDI Fund (TKP2020 NC: Grant No. BME-NCS and TAK2021: project no. BME-NVA-02) based on the charter of bolster issued by the NRDI Office under the auspices of the Ministry for Innovation and Technology.

REFERENCES

[1] Tavakoli, M., Tavakoli, A., Taheri, M., Saghafifar, H., 2012, „Design, simulation and structural optimization of a longitudinal acoustic resonator for trace gas detection using laser photoacoustic spectroscopy (LPAS)", *Opt. Laser Technol.*, Vol. 42, pp. 828-838

[2] Gong, Z., Chen, K. Chen, Y., Mei, L., Yu, Q., 2019, "Integration of T-type half open photoacoustic cell and fiber-optic acoustic sensor for trace gas detection", *Opt. Express*, Vol. 27, pp. 18222-18231

[3] Gliére, A., Rouxel, J., Parvitte, B., Boutami, S., Zéninari, V., 2013, "A coupled model for the simulation of miniaturized and integrated photoacoustic gas detector", *Int. J. Thermophys.*, Vol. 34, pp. 2119-2135.

[4] El-Busaidya, S. A. S., Baumann, B., Wolff, M., Duggen, L., 2020, „Modelling of open photoacoustic resonators", *Photoacoustics*, Vol. 18, 100161.

[5] Bozóki, Z., Szabó, A., Mohácsi, Á., and Szabó, G., 2010, "A fully opened photoacoustic resonator based system for fast response gas concentration measurements", *Sensors and Actuators B: Chemical*, Vol. 147, pp. 206-212.

[6] Miklós, A., Schäfer, S., and Hess, P., 1999, "Photoacoustic Spectroscopy, Theory", *Encyclopedia Of Spectroscopy And Spectrometry*, pp. 1815-1822.

[7] Dumitras, D.C., Dutu, D.C., Matei, C., Magureanu, A. M., Petrus, M., and Popa, C., 2007, "Laser photoacoustic spectroscopy: principles, instrumentation, and characterization", *Journal of Optoelectronics and Advanced Materials*, Vol. 9(12), pp. 3655 – 3701.

[8] Baumann, B., Kost, B., Wolff, M., and Groninga, H., 2008, "Modeling and Numerical Investigation of Photoacoustic Resonators", *In: Modelling and Simulation*, IntechOpen, pp. 17-38.

[9] Kost, B., Baumann, B., Germer, M., Wolf, M., 2009, "Shape Optimization of Photoacoustic Resonators", *In: Computer Aided Optimum Design in Engineering XI*, Wessex Institute of Technology, pp. 45-54.

[10] Geuzaine, C. and Remacle, J.-F., 2009, "Gmsh: a three-dimensional finite element mesh generator with built-in pre- and post-processing facilities", *International Journal for Numerical Methods in Engineering*, Vol. 79(11), pp. 1309–1331.

[11] Weller, H. G., Tabor, G., Jasak, H., Fureby, C., 1998, "A tensorial approach to computational continuum mechanics using object-oriented techniques", *Computers In Physics*, Vol. 12, No. 6., pp 620–631

[12] Poletto, R., Craft, T., and Revell, A., 2013, "A New Divergence Free Synthetic Eddy Method for the Reproduction of Inlet Flow Conditions for LES". *Flow, Turbulence and Combustion*, Vol. 91, No. 3, pp. 519–539